ACS APPLIED MATERIALS & INTERFACES

Research Article

Cite This: ACS Appl. Mater. Interfaces 2017, 9, 43739−43746

www.acsami.org

Organic Photosensitizers Incorporating Rigid Benzo[1,2-*b*:6,5-*b*′]dithiophene Segment for High-Performance Dye-Sensitized Solar Cells

Chun-Ting Li,[†] Feng-Ling Wu,[†] Bing-Hsuan Lee,[†,‡] Ming-Chang P. Yeh,*[,‡] and Jiann T. Lin*[,†]

[†]Institute of Chemistry, Academia Sinica, No. 128, Section 2, Academia Road, Nankang District, Taipei 11529, Taiwan

[‡]Department of Chemistry, National Taiwan Normal University, 117 Taipei, Taiwan

Supporting Information

ABSTRACT: Benzo[1,2-*b*:6,5-*b*′]dithiophene (**BDT**) entity with rigid skeleton is introduced into the conjugated spacer of organic dyes, with triphenylamine as the electron donor and 2-cyanoacrylic acid as the acceptor, have been prepared for dye-sensitized solar cells. Inserting an aromatic entity between **BDT** and the anchor extends the absorption wavelength of the dyes and improves the dark current suppression efficiency, and consequently leads to better cell performance. Addition of chenodeoxycholic acid coadsorbent alleviates dye aggregation and results in better cell efficiency. The dye inserted with 4*H*-cyclopenta[2,1-*b*:3,4-*b*′]dithiophene entity achieves the best efficiency (9.11%) when I^-/I_3^- was used as the electrolyte. When $Co(phen)_3^{2+/3+}$ was used as the electrolyte, the efficiency further boosts to 9.88%.

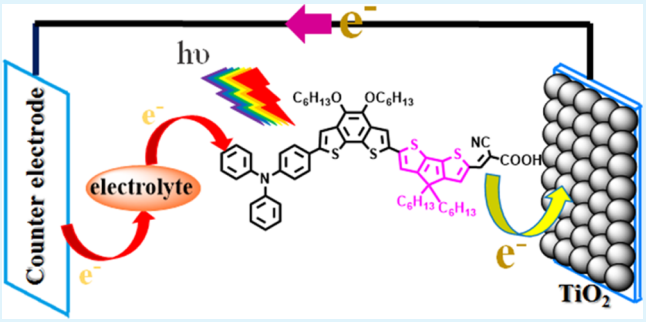

KEYWORDS: *dye-sensitized solar cell, metal-free sensitizers, benzo[1,2-b:6,5-b′]dithiophene, cobalt electrolyte, coadsorbent*

1. INTRODUCTION

Solar power as an alternative of fossil fuels and nuclear energy for human energy demand is deemed promising because of its unlimited supply and environmental friendliness. As an emerging photovoltaic technology, dye-sensitized solar cells (DSSCs) have attracted widespread interest after O'Regan and Grätzel's[1] seminal work because they own advantages of low cost, facile fabrication, and high efficiency.[2−5] Currently, DSSCs have performance approaching that of amorphous silicon solar cell. In addition, DSSCs compete favorably with other solar cell technologies under dim or diffuse light condition, and are particularly promising for indoor applications,[6,7] such as powering portable electronics. There are three prototype sensitizers, ruthenium pyridine complexes, porphyrin dyes, and metal-free dyes; the best efficiencies of the pertinent DSSCs based on single sensitizer have reached 11.5,[8] 13.0,[9] and 13.0%,[10] respectively. The efficiency even reached 14.3% for a cell using two metal-free dyes.[11] We have persistent interest in sensitizers, as they are critical to the cell performance, and high performance should be important for future commercialization. Among metal-free sensitizers with D−π−A (D = electron donor; π = π-conjugated spacer; A = acceptor) configuration, those with a fused aromatic spacer[12] are interesting because the rigid spacer has a smaller reorganization energy, which favors electronic communication of the donor with the acceptor. Very recently, we developed a series of metal-free dyes having a rigidified conjugated segment comprising fused electron-deficient and electron-rich aromatics, including dithieno-[3′,2′:3,4;2″,3″:5,6]-benzo[1,2-*c*][1,2,5]oxadiazole,[13] dithieno-[3,2-*f*:2′,3′-*h*]quinoxaline,[13,14] and dithieno[3,2-*b*]-pyrrolobenzo-triazole.[15,16] DSSCs based on these sensitizers exhibit good conversion efficiencies, as the dyes possess strong and broad absorption. Benzo[1,2-*b*:6,5-*b*′]dithiophene (**BDT**), composed of fused bithienyl entity and phenyl entity, is the common structural motif of the aforementioned rigidified segments. In view of complicated synthetic procedures of the aforementioned rigidified segments, we decided to replace these segments with **BDT**, as several metal-free dyes with a fused aromatic spacer exhibit good potential for high-performance DSSCs.[12]

Benzo[1,2-*b*:4,5-*b*′]dithiophene, an isomer of **BDT** unit, is among the most popular donor units for semiconducting polymers with good photovoltaic properties because its rigid and planar structure is beneficial to easier π−π stacking as well as hole mobility.[17−21] Benzo[1,2-*b*:4,5-*b*′]dithiophene unit was also used in the sensitizers of DSSCs.[22] Another **BDT** isomer, benzo[1,2-*b*:4,3-*b*′]-dithiophene, was also reported for DSSC application.[23] To our knowledge, benzo[1,2-*b*:6,5-*b*′]-dithiophene (**BDT**), has not been incorporated in the spacer of sensitizers so far. Different highest occupied molecular orbital (HOMO) and lowest unoccupied molecular orbital (LUMO) levels between benzo[1,2-*b*:6,5-*b*′]dithiophene (Fig-

Received: October 6, 2017
Accepted: November 28, 2017
Published: November 28, 2017

DOI: 10.1021/acsami.7b15181
ACS Appl. Mater. Interfaces 2017, 9, 43739−43746

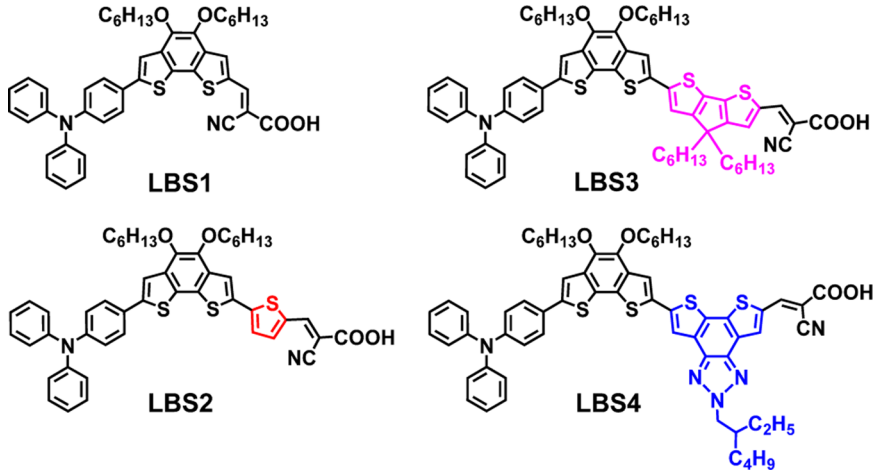

Figure 1. Molecular structures of **BDT(Ohex)$_2$** dyes (**LBS1−4**).

Scheme 1. Synthetic Routes of the LBS Dyes[a]

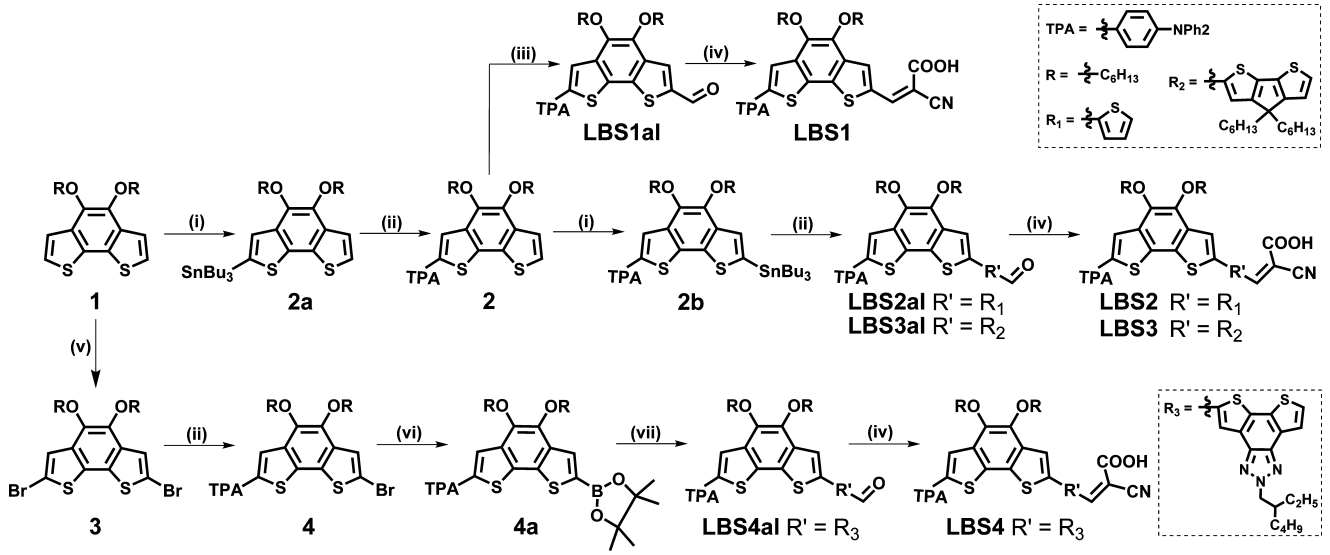

[a](i) Lithium diisopropylamide (LDA), $SnBu_3Cl$, −78 °C, 18 h; (ii) bis(triphenylphosphine)palladium(II) dichloride ($Pd(PPh_3)_2Cl_2$), dimethylformamide (DMF), 60 °C, 18 h; (iii) LDA, DMF, −78 °C, 18 h; (iv) cyanoacetic acid, ammonium acetate (NH_4OAc), acetic acid (AcOH), 120 °C; (v) *N*-bromosuccinimide, CH_2Cl_2, 18 h; (vi) bis(pinacolato)diboron, potassium acetate (KOAc), $PdCl_2$(dppf) (where dppf = 1,1′-bis(diphenylphosphino)ferrocene), 1,4-dioxane, 120 °C, 20 h; (vii) tetrakis(triphenylphosphine)palladium(0) ($Pd(PPh_3)_4$), 2M K_2CO_3, toluene, 120 °C, 20 h.

ure S1; HOMO: −5.59 eV; LUMO: −0.94 eV) and benzo[1,2-*b*:4,3-*b*′]dithiophene (Figure S1; HOMO: −5.38 eV; LUMO: −0.89 eV) entities may lead to different electronic effect when used as the conjugated bridge. We therefore set up to synthesize new sensitizers containing benzo[1,2-*b*:6,5-*b*′]-dithiophene (**BDT**) in the spacer. We were aware that benzo[1,2-*b*:6,5-*b*′]dithiophene with two alkoxy substituents at the phenyl ring can be prepared in good yield.[24] Compared with a bithiophene entity, the two thiophene rings in **BDT** unit reside in the same plane, which can better benefit electronic communication of their peripheral π-segments. Moreover, incorporation of the alkoxy substituents in **BDT** may help the dyes with solubility enhancement in common organic solvents,[25,26] and dark current suppression as well.[27,28] There are some reports on sensitizers with coplanar bithiophene rings, such as 4,4-disubstituted 4*H*-cyclopenta[2,1-*b*:3,4-*b*′]-dithiophene,[29,30] 3,3′-disubstituted silylene-2,2′-bithiophene,[31−33] dithieno[3,2-*b*;2′,3′-*d*]thiophene,[34] naphtho[2,1-*b*:3,4-*b*′]dithiophene,[35] and dithieno[3,2-*b*:2′,3′-*d*]pyrrole.[36] Many of these sensitizers exhibit good cell performance. Herein, we report the new dyes and high-performance DSSCs using the new **BDT**-based dyes as sensitizers.

2. RESULTS AND DISCUSSION

2.1. Preparation of BDT Sensitizers. 4,5-Bis(hexyloxy)-benzo[1,2-*b*:6,5-*b*′]dithiophene (abbreviated as **BDT(Ohex)$_2$**) was prepared following the method of Reynolds et al.,[24] with the incorporation of hexyloxy chains for better solubility of the dyes in organic solvents. Figure 1 shows the structures of new **BDT(Ohex)$_2$**-based sensitizers (**LBS1−4**), and Scheme 1 illustrates their synthetic routes. Conversion of **BDT(Ohex)$_2$** to stannyl derivative, followed by palladium-catalyzed Stille coupling with arylamine, led to the incorporation of the arylamine donor. The intermediate **2** could be formylated directly or via reaction with Stille coupling with appropriate

DOI: 10.1021/acsami.7b15181
ACS Appl. Mater. Interfaces 2017, 9, 43739−43746

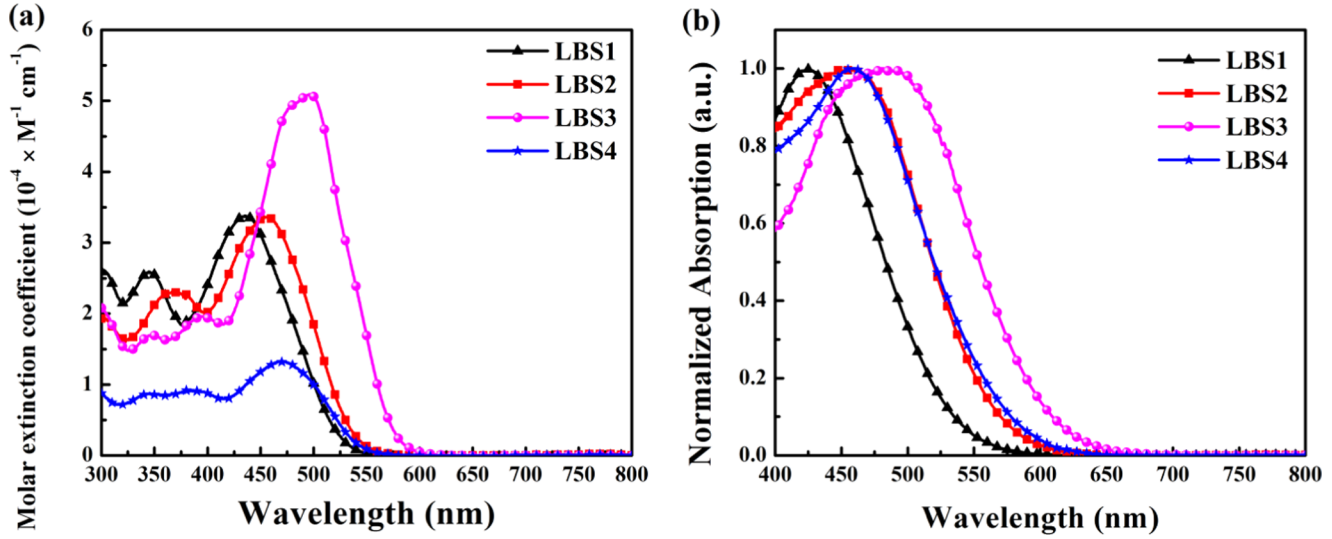

Figure 2. Absorption spectra of **LBS** dyes (a) dissolved in THF (0.1 mM, 10^{-3} mmol in 10 mL of THF) and (b) adsorbed on TiO_2 film (4 μm).

Table 1. Photophysical and Electrochemical Data of the LBS Dyes[a]

dye	λ_{abs}^{THF} (nm) (ε × 10^{-4} M^{-1} cm^{-1})	λ_{em} (nm)	λ_{0-0} (nm)	E_{0-0} (eV)[b]	λ_{abs}^{film} (nm)[c]	λ_{onset}^{film} (nm)[c]	HOMO/LUMO (eV)	E_{OX} (V)[d]	E_{0-0}* (V)[e]
LBS1	435 (3.38)	551	498	2.49	425	575	5.74/3.25	1.34	−1.15
LBS2	456 (3.35)	563	511	2.42	457	617	5.70/3.28	1.30	−1.12
LBS3	497 (5.09)	574	528	2.35	477	650	5.69/3.34	1.29	−1.06
LBS4	470 (1.32)	551	511	2.42	459	623	5.68/3.26	1.28	−1.14

[a]Based on THF solution at 298 K. [b]Calculated via E_g^{opt} = 1240/λ_{0-0}, where λ_{0-0} is read from the cross point of absorption and emission spectra. [c]Based on 4 μm thick TiO_2 film. [d]Adjusted to be vs to normal hydrogen electrode (NHE) using ferrocene/ferrocenium as an internal reference. [e]Calculated via E_{0-0}* = E_{OX} − E_{0-0} (vs NHE).

aromatic segment (thienyl ring for **LBS2** and 4*H*-cyclopenta-[2,1-*b*:3,4-*b*′]dithiophene for **LBS3**) containing formyl group. Finally, Knoevenagel condensation of the formyl intermediates (**LBS1al**−**3al**) with cyanoacetic acid afforded **LBS1**−**3**. On the other hand, **LBS4** was obtained from palladium-catalyzed Stille coupling of dibrominated **BDT(Ohex)$_2$** with stannylated arylamine, followed by palladium-catalyzed Suzuki coupling with dithieno[3′,2′:3,4;2″,3″:5,6]-benzo[1,2-*d*][1,2,3]triazole segment containing formyl group and Knoevenagel condensation.

2.2. Photophysical and Electrochemical Characteristics. UV−vis absorption spectra of **LBS** sensitizers dissolved in tetrahydrofuran (THF) (0.1 mM, 10^{-3} mmol in 10 mL of THF) and adsorbed on the TiO_2 film (4 μm) are presented in Figure 2a,b, respectively. Table 1 compiles the corresponding photophysical data. The absorption maximum (λ_{abs}^{THF}) of the intramolecular charge transfer (ICT) transition in these dyes ranges from 416 to 497 nm, with the molar extinction coefficient (ε) in the range of 13 200−50 900 M^{-1} cm^{-1}. The λ_{abs}^{THF} value increases as the conjugation length increases: **LBS1** < **LBS2** < **LBS4** < **LBS3**. The significantly lower ε value of **LBS4** compared with others may be attributed to the electron accumulation of its LUMO at the nitrogen atoms on the benzotriazole entity (vide infra); this phenomenon results in smaller orbital overlap between the HOMO and LUMO. The **LBS** dye has a longer wavelength absorption onset on TiO_2 film than in the solution, indicating the presence of significant *J*-aggregation of the dyes except **LBS1**.[37] Dye aggregation was also checked with the **LBS** dyes on TiO_2 film with addition of chenodeoxycholic acid (CDCA),[38] as shown in Figure S2. There is nearly no shift of the absorption for the **LBS1** with the addition of CDCA up to 30 mM (0.1−0.3 mmol in 10 mL of the dye solution). In contrast, other dyes with longer π-spacer exhibit blue shift of the absorption when CDCA was added. There is more sluggish spectral response for **LBS4**, implying its more serious dye aggregation. It is interesting to note that **LBS1** has a larger λ_{abs} (476 nm; Figure S3) in CH_2Cl_2 than its benzo[1,2-*b*:4,3-*b*′]-dithiophene congener (Figure S4), **G55** (459 nm),[23] even though the arylamine of the latter has two electron-donating hexyloxy substituents. The carboxylic acid of dye **G55** may have a higher degree of deprotonation in CH_2Cl_2, which leads to hypsochromic shift of the spectra.[39,40] There is only weak emission for all **LBS** dyes in the solution.

The cyclic voltammograms of the **LBS** sensitizers (1 mM, 10^{-2} mmol in 10 mL of THF) are shown in Figure S5, and Table 1 compiles the corresponding data. One quasi-reversible one-electron oxidation wave at 1.28−1.34 V more positive than normal hydrogen electrode (NHE) is ascribed to the electron removal at the arylamine donor. The potentials of **LBS2**−**4** are slightly lower than that of **LBS1** due to additional thiophene rings in the conjugated spacer. The more positive oxidation potential of the arylamine than the iodide/triiodide redox couple (0.4 V vs NHE)[41] indicates an energetically favorable dye regeneration. The excited state potential (E_{0-0}*) of the dye was calculated from the difference between the first oxidation potential (E_{OX}) and the zero−zero excitation energy (E_{0-0}), with the latter obtained from the intersection of the normalized UV−vis absorption and photoluminescence spectra (Figure S6). The E_{0-0}* values (−1.06 to −1.15 V vs NHE) indicate

DOI: 10.1021/acsami.7b15181
ACS Appl. Mater. Interfaces 2017, 9, 43739−43746

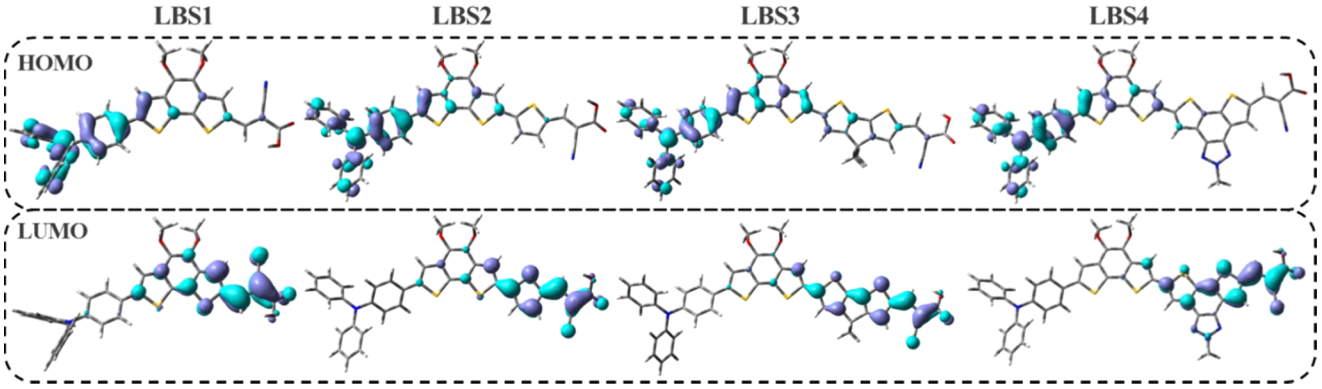

Figure 3. Selected frontier molecular orbitals of the **LBS** dyes.

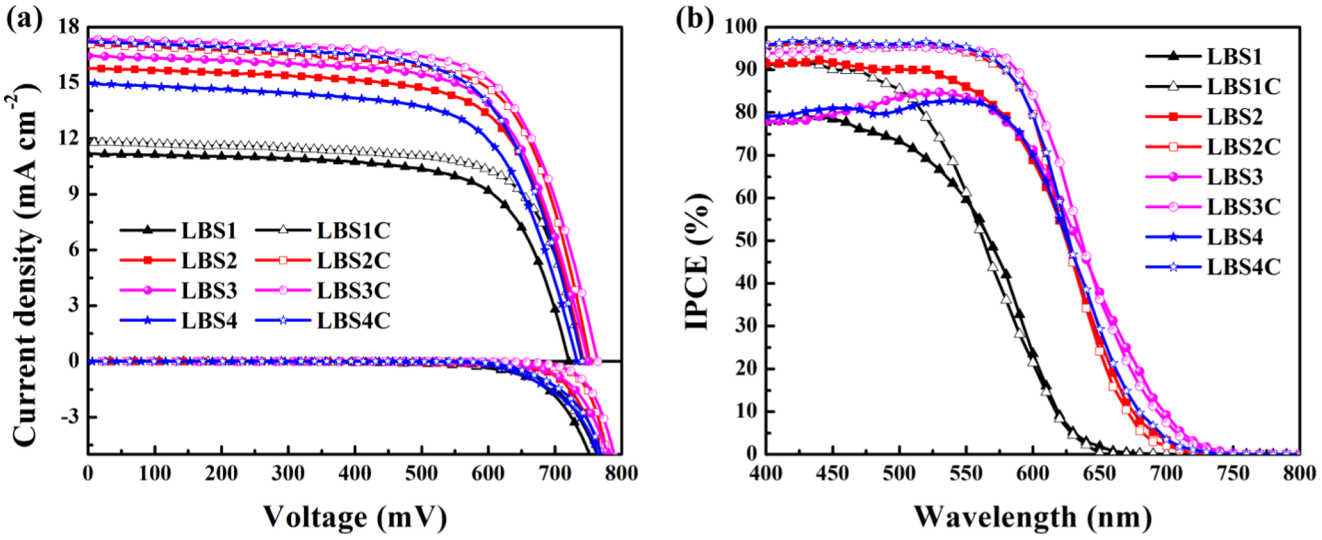

Figure 4. (a) Current density−voltage curves and (b) incident photon-to-current conversion efficiency spectra for the DSSCs with the **LBS** dyes, measured in an I^-/I_3^- electrolyte under a simulated AM 1.5G illumination, dark condition, or monochromatic incident light illumination.

energetically favorable electron injection from the excited dye into the conduction band of TiO_2 (conduction band edge: −0.5 V vs NHE).[42]

2.3. Density Functional Theory (DFT) Calculations. Density functional theory (DFT) and time-dependent DFT calculations were performed (see details in the Supporting Information) for a better insight into the molecular structures of the dyes versus the performance of DSSCs; the correlated data are summarized in Table S1. Figures 3 and S7 show the selected frontier orbitals. The π-electron in the highest occupied molecular orbital (HOMO) of **LBS** dyes largely distributes at triphenylamine donor and slightly extended to the **BDT** core. In comparison, the π-electron of the lowest unoccupied molecular orbital (LUMO) mainly resides at cyanoacrylic acid (**Ac**) and extends to the neighboring heteroaromatic rings. The contribution of the **BDT** core to the LUMO in **LBS2**−**4** is significantly smaller compared with **LBS1**. In the case of **LBS4**, the electron in its LUMO (Figure 3) is partially accumulated at the benzotriazole entity, resulting in the unfavorable electron-trapping and photophysical properties (vide supra).

In Table S1, the lowest energy transition, $S_0 \rightarrow S_1$, for all **LBS** dyes is nearly 100% of HOMO → LUMO, and therefore has prominent charge-transfer character. The successful intramolecular charge transfer is also supported via the dihedral angle diagram of **LBS** dyes (Figure S8). At the ground state, the dihedral angle between **BDT** and the arylamine ranges from 18 to 25°, and that between **BDT** and thiophene ring ranges from 4 to 7°. The more intense electronic absorption in **LBS3** than others is supported by its larger computed oscillation strength (*f*) and significant orbital overlap between the HOMO and LUMO. Moreover, Mulliken charges variation during electronic transition (Table S1) for all **LBS** dyes were estimated via dividing the dye molecules into several segments: the donor group (**TPA**), **BDT** (**BDT**(**Ohex**)$_2$), the acceptor group (cyanoacrylic acid, **Ac**), and the heteroaromatic entity (**Het**) connected to **Ac**. Figure S9 shows the Mulliken charges variations between the two excited states (S_1 and S_2) and the ground state (S_0). For the $S_0 \rightarrow S_1$ transition, the **BDT** entity has a significant negative charge when it is directly connected to the acceptor (**LBS1**). In comparison, the charge is negligible when a thienyl ring is used as the **Het** (**LBS2**), and positive when **Het** is 4*H*-cyclopenta[2,1-*b*:3,4-*b*′]dithiophene (**LBS3**) or dithieno-[3′,2′:3,4;2″,3″:5,6]benzo[1,2-*d*][1,2,3]triazole (**LBS4**). For the $S_0 \rightarrow S_2$ transition, the **BDT** entity acts as the second electron donor. We also carried out computation on **G55**′ (Figure S4), derived from **G55** (Figure S4)[23] with 4,5-bis(hexyloxy)benzo[1,2-*b*:6,5-*b*′]dithiophene replaced by 4,5-bis(metoxy)benzo[1,2-*b*:6,5-*b*′]dithiophene and omission of the alkoxy chain at the donor. Compared with **LBS1**, we

DOI: 10.1021/acsami.7b15181
ACS Appl. Mater. Interfaces 2017, 9, 43739−43746

Table 2. Photovoltaic Parameters for the DSSCs with Various LBS Dyes, Measured at AM 1.5G Based on Five Cells in the I^-/I_3^- Electrolyte[a]

	dye	η (%)	V_{OC} (mV)	J_{SC} (mA cm^{-2})	FF	DL × 10^{-7} (mol cm^{-2})	R_{rec} (Ω)	τ_e (ms)
without CDCA	**LBS1**	5.57 ± 0.15	721.00 ± 7.75	11.16 ± 0.04	0.69 ± 0.00	1.43	195.39	15.31
	LBS2	8.01 ± 0.07	739.17 ± 2.04	15.83 ± 0.14	0.68 ± 0.00	1.12	239.17	20.11
	LBS3	8.38 ± 0.04	743.75 ± 2.50	16.46 ± 0.08	0.68 ± 0.00	1.28	339.10	26.43
	LBS4	7.30 ± 0.13	728.00 ± 2.74	15.04 ± 0.27	0.67 ± 0.00	2.63	203.84	15.31
with 10 mM CDCA	**LBS1C**	6.21 ± 0.04	739.96 ± 4.09	11.81 ± 0.04	0.71 ± 0.00	0.80	240.84	20.11
	LBS2C	8.84 ± 0.02	750.00 ± 0.00	17.08 ± 0.03	0.69 ± 0.00	0.40	363.51	26.43
	LBS3C	9.11 ± 0.00	762.50 ± 2.89	17.36 ± 0.02	0.69 ± 0.00	0.70	355.61	26.43
	LBS4C	8.44 ± 0.07	738.00 ± 2.74	17.17 ± 0.23	0.67 ± 0.01	0.88	238.00	20.11

[a]The cell having CDCA as the coadsorbent for **LBS** dyes were denoted as **LBS1C**, **LBS2C**, **LBS3C**, and **LBS4C**. DL means the dye loading amount on the TiO_2 film for DSSC. The 10 mM of CDCA indicates 0.1 mmol of CDCA added into 10 mL of the dye solution.

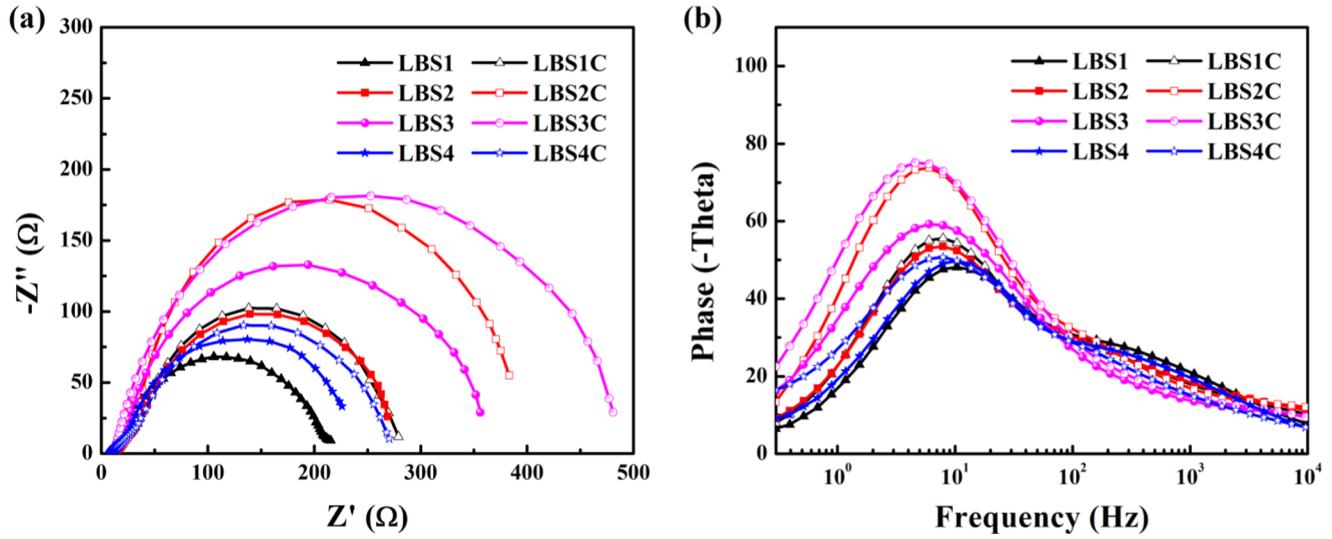

Figure 5. Electrochemical impedance spectra for the DSSCs with the **LBS** dyes: (a) Nyquist and (b) Bode plots, measured in an I^-/I_3^- electrolyte under dark with an applied bias of −0.70 V.

found no significant difference in the dihedral angles between different segments (Figure S8) and the energy of the $S_0 \rightarrow S_1$ transition (Table S1).

2.4. Photovoltaic Performance of DSSCs Based on LBS Sensitizers. The DSSCs of **LBS** dyes were obtained under a simulated AM 1.5G (100 mW cm^{-2}) illumination in an iodide-based (I^-/I_3^-) electrolyte. Figure 4a,b shows the current density−voltage (J−V) curves and incident photon-to-current conversion efficiency (IPCE) spectra (400−800 nm), respectively, and Table 2 compiles the related cell performance data. The dye having a conjugated entity, thienyl ring (**LBS2**, 8.01%), 4*H*-cyclopenta[2,1-*b*:3,4-*b*′]dithiophene (**LBS3**, 8.38%) or dithieno[3′,2′:3,4;2″,3″:5,6]-benzo[1,2-*d*][1,2,3]-triazole (**LBS4**, 7.30%), between the anchor and **BDT** has higher J_{SC}, V_{OC}, and thus η than **LBS1** (5.57%). The decreasing order of the J_{SC} value, **LBS3** > **LBS2** > **LBS4** > **LBS1**, is in agreement with the absorption spectra of the dyes on TiO_2 (Figure 2b). Although the ε value of **LBS4** is the least, the high J_{SC} value of **LBS4** can be attributed to its high dye loading (Table 2) and wide absorption range on the TiO_2 film. The V_{OC} values also decrease in the same order, which is in opposite trend of dark currents (vide infra); the possible influence of conduction band edge shift of TiO_2 and dye aggregation on V_{OC} cannot be ruled out, however. The best device performance of **LBS3** certainly is benefited from the best light absorption and sufficient dark current suppression (vide infra) due to the presence of 4*H*-cyclopenta[2,1-*b*:3,4-*b*′]dithiophene. In the case of **LBS4**, which has a longer λ_{abs}^{THF} than **LBS2**, the electron-trapping in the triazole entity and more severe dye aggregation may lead to the lower J_{SC} and V_{OC} values than for **LBS2**. The benzo[1,2-*b*:4,3-*b*′]-dithiophene congener (**G55**; Figure S4) was reported to have an efficiency (η) of 5.6%, V_{OC} of 810 mV, J_{SC} of 9.4 mA cm^{-2}, and fill factor (FF) of 0.74.[23] In comparison with **G55**, **LBS1** has the same cell conversion efficiency (5.6%), but lower V_{OC} and higher J_{SC} values. Possibly, the two additional alkoxy chains at the donor of the former help with suppressing dark current,[43,44] whereas the latter has better light harvesting (vide supra).

Chenodeoxycholic acid (CDCA) is commonly used as the coadsorbent to break the dye aggregation and/or suppress the dark current.[45] DSSCs with CDCA and **LBS** dyes were thus investigated and denoted as **LBS1C**, **LBS2C**, **LBS3C**, and **LBS4C**. Figure 4 shows the J−V curves and IPCE spectra, and Table 2 summarizes the corresponding performance data of the DSSCs. In spite of lower dye-loading, DSSCs containing CDCA still provide higher J_{SC} and V_{OC} values than those of the cells without CDCA. It suggested that CDCA helps with antiaggregation of **LBS** dyes. Moreover, better dark current suppression is achieved via applying CDCA, as evidenced from the dark current density−voltage curves shown in the lower part of Figure 4a: the cells with CDCA shows obviously lower dark currents. With the addition of CDCA, the cell efficiencies

DOI: 10.1021/acsami.7b15181
ACS Appl. Mater. Interfaces 2017, 9, 43739−43746

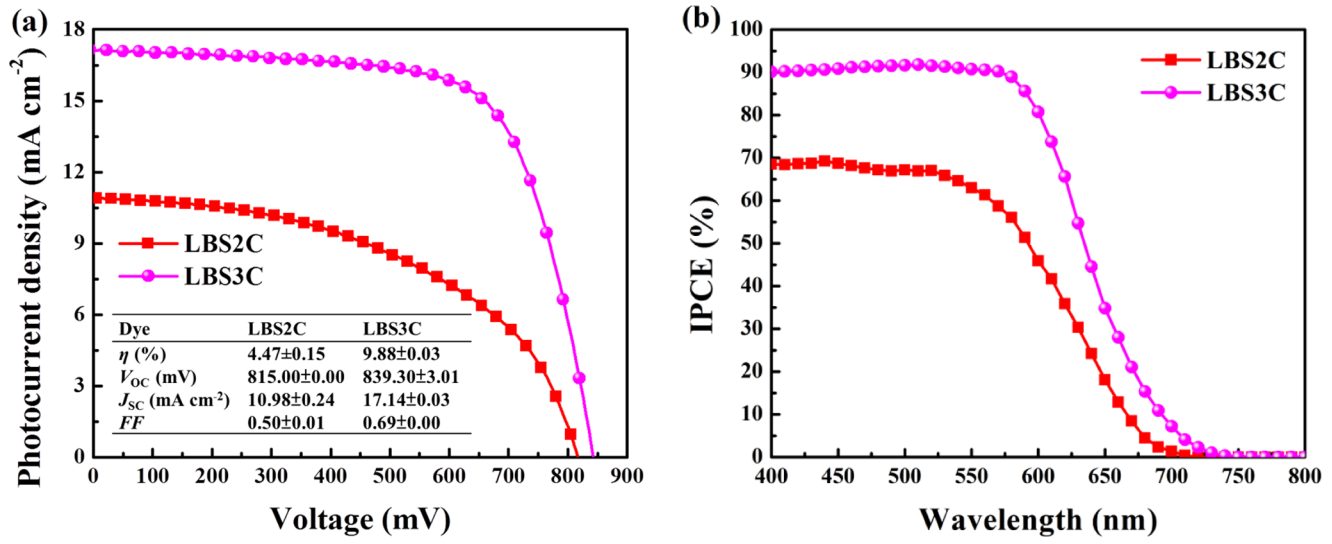

Figure 6. (a) Photocurrent density−voltage curves and (b) incident photon-to-current conversion efficiency spectra of the DSSCs with **LBS2C** and **LBS3C** dyes, measured in a Co^{2+}/Co^{3+} electrolyte under a simulated AM 1.5G illumination. The cobalt-based electrolyte contains 0.35 M $[Co(phen)_3](TFSI)_2$, 0.05 M $[Co(phen)_3](TFSI)_3$, 0.8 M TBP, and 0.1 M lithium perchlorate ($LiClO_4$) in acetonitrile (phen = 1,10-phenanthroline; TFSI = bis(trifluoromethane)sulfonimide).

for **LBS2C**, **LBS3C**, and **LBS4C** reach 8.84, 9.11, and 8.44%, respectively, which are much higher than the efficiency of **LBS1C** (6.21%) and competitive with that of the N719-based standard cell (8.44%; Figure S10).

For the cells without and with CDCA, the absorption edges of the IPCE spectra for all of the **LBS** dyes follow the same order with their absorption spectra, **LBS3** > **LBS2** ≈ **LBS4** > **LBS1**. The IPCE values for all of the **LBS** dyes are increased upon the addition of CDCA, which further substantiates the successful alleviation of dye aggregation by CDCA. Besides, the cell with CDCA shows a minor blue shift compared with the cells without CDCA; this phenomenon is in good agreement with their absorption spectra based on the TiO_2 thin film (vide supra).

2.5. Electrochemical Impedance Spectra (EIS) Analysis. The EIS of DSSCs using an iodide-based electrolyte were recorded under dark condition by applying a voltage of −0.70 V, and used to evaluate the dark current suppression ability of the **LBS** dyes. Accordingly, the charge recombination resistance (R_{rec}) and electron recombination lifetime (τ_e^{dark}) at the photoanode/electrolyte interface were calculated via the pertinent Nyquist (Figure 5a) and Bode (Figure 5b) plots, as shown in Table 2.[46] The values of R_{rec} and τ_e^{dark} decrease in the order of **LBS3** (339.10 Ω, 26.43 ms) > **LBS2** (239.17 Ω, 20.11 ms) > **LBS4** (203.84 Ω, 15.31 ms) > **LBS1** (195.39 Ω, 15.31 ms). Insertion of an aromatic entity between **BDT** and the anchor obviously benefits dark current suppression. It is notable that the V_{OC} values, dark currents, R_{rec}, and τ_e^{dark}, though obtained from different measurement techniques, are in line with one another. With added CDCA, the values of R_{rec} and τ_e^{dark} decrease in the order of **LBS2** (363.51 Ω, 26.43 ms) ≈ **LBS3** (355.61 Ω, 26.43 ms) > **LBS1** (240.84 Ω, 20.11 ms) ≈ **LBS4** (238.00 Ω, 20.11 ms). Although increased R_{rec} and τ_e^{dark} values implies that CDCA may help with suppressing the dark current, the significantly increased IPCE values (vide supra) suggest that alleviation of dye aggregation may play a more important role. This is especially true for **LBS4**, which has a significant drop in dye-loading amount and improved J_{SC} value after adding CDCA.

2.6. LBS-Based DSSCs Using Cobalt-Based Electrolyte. In contrast with I^-/I_3^-, cobalt redox mediator has negligible absorption in the visible-light region. Moreover, its higher redox potential has a high potential for higher photovoltage, and therefore better cell performance.[47−49] Cobalt-based redox mediator, $Co(phen)_3^{2+/3+}$ (phen = 1,10-phenanthroline), was thus tested for **LBS2** and **LBS3** with CDCA (see details in the Supporting Information). For the cell of **LBS3**, the V_{OC} value (839.30 mV) was raised by ∼77 mV, and thus the conversion efficiency was boosted to 9.88%. The $J-V$ curves and IPCE spectra (400−800 nm) are shown in Figure 6a,b, respectively, and the performance data of the cells are summarized in the inset table of Figure 6a. Although **LBS2**-based cell also has a higher V_{OC} value of 839.30 mV (65 mV increment), the conversion efficiency drops to 4.47% due to a significant drop in J_{SC} value. The lower J_{SC} values may be stemmed from the mass transport limit of the cobalt electrolyte and severe charge recombination with the Co^{3+} redox mediator.[50] Accordingly, it may be deduced that **LBS2** possesses sufficient suppression for I_3^- recombination and thus gives its iodide-based cell good J_{SC} and FF values. However, **LBS2** is insufficient to retard Co^{3+} recombination, which is much more serious than that for I_3^-, leading to poor J_{SC} and FF values.

3. CONCLUSIONS

New dipolar sensitizers incorporating 4,5-bis(hexyloxy)benzo-[1,2-*b*:6,5-*b*′]dithiophene entity (**BDT(Ohex)$_2$**) in the π-bridge between arylamine donor and 2-cyanoacrylic acid acceptor have been prepared and used for DSSCs. Upon further incorporation of a heteroaromatic segment between **BDT(Ohex)$_2$** and the acceptor, the light harvesting of the dyes increases. Consequently, the conversion efficiencies of the DSSCs using I^-/I_3^- redox mediator reached 7.3−8.4% without CDCA and 8.4−9.1% with CDCA coadsorbent, respectively. The efficiency of the best cell was further boosted to 9.88% using $Co(phen)_3^{2+/3+}$ redox mediator.

DOI: 10.1021/acsami.7b15181
ACS Appl. Mater. Interfaces 2017, 9, 43739−43746

■ ASSOCIATED CONTENT

Supporting Information

The Supporting Information is available free of charge on the ACS Publications website at DOI: 10.1021/acsami.7b15181.

Complete experimental details and spectroscopy data, ^{1}H and ^{13}C NMR of all of the new dyes, and details of the theoretical calculation (PDF)

■ AUTHOR INFORMATION

Corresponding Authors

*E-mail: cheyeh@ntnu.edu.tw (M.-C.P.Y.).
*E-mail: jtlin@gate.sinica.edu.tw (J.T.L.).

ORCID

Ming-Chang P. Yeh: 0000-0003-2963-5707
Jiann T. Lin: 0000-0002-9704-5322

Author Contributions

The manuscript was written through contributions of all of the authors. All of the authors have given approval to the final version of the manuscript.

Notes

The authors declare no competing financial interest.

■ ACKNOWLEDGMENTS

We acknowledge the Support (Technology Development for Deep Decarbonization: grant no. 106-0210-02-11-03) of the Academia Sinica (AS), the Ministry of Science and Technology of Taiwan, and Instrumental Center of Institute of Chemistry, AS. We are also grateful to the program "Technology Development for Deep Decarbonization" (grant no. 106-0210-02-11-03).

■ REFERENCES

(1) O'Regan, B.; Grätzel, M. A Low-Cost, High-Efficiency Solar Cell Based on Dye-Sensitized Colloidal TiO_2 Films. *Nature* **1991**, *353*, 737−740.

(2) Hagfeldt, A.; Boschloo, G.; Sun, L.; Kloo, L.; Pettersson, H. Dye-Sensitized Solar Cells. *Chem. Rev.* **2010**, *110*, 6595−6663.

(3) Yen, Y.-S.; Chou, H.-H.; Chen, Y.-C.; Hsu, C.-Y.; Lin, J. T. Recent Developments in Molecule-Based Organic Materials for Dye-Sensitized Solar Cells. *J. Mater. Chem.* **2012**, *22*, 8734−8747.

(4) Ooyama, Y.; Harima, Y. Photophysical and Electrochemical Properties, and Molecular Structures of Organic Dyes for Dye-Sensitized Solar Cells. *ChemPhysChem* **2012**, *13*, 4032−4080.

(5) Albero, J.; Atienzar, P.; Corma, A.; Garcia, H. Efficiency Records in Mesoscopic Dye-Sensitized Solar Cells. *Chem. Rec.* **2015**, *15*, 803−828.

(6) Freitag, M.; Teuscher, J.; Saygili, Y.; Zhang, X.; Giordano, F.; Liska, P.; Hua, J.; Zakeeruddin, S. M.; Moser, J.-E.; Grätzel, M.; Hagfeldt, A. Dye-Sensitized Solar Cells for Efficient Power Generation under Ambient Lighting. *Nat. Photonics* **2017**, *11*, 372−378.

(7) Tingare, Y. S.; Vinh, N. S.; Chou, H.-H.; Liu, Y.-C.; Long, Y.-S.; Wu, T.-C.; Wei, T.-C.; Yeh, C.-Y. New Acetylene-Bridged 9,10-Conjugated Anthracene Sensitizers: Application in Outdoor and Indoor Dye-Sensitized Solar Cells. *Adv. Energy Mater.* **2017**, *7*, No. 1700032.

(8) Chen, C.-Y.; Wang, M.; Li, J.-Y.; Pootrakulchote, N.; Alibabaei, L.; Ngoc-le, C.-h.; Decoppet, J.-D.; Tsai, J.-H.; Grätzel, C.; Wu, C.-G.; Zakeeruddin, S. M.; Grätzel, M. Highly Efficient Light-Harvesting Ruthenium Sensitizer for Thin-Film Dye-Sensitized Solar Cells. *ACS Nano* **2009**, *3*, 3103−3109.

(9) Mathew, S.; Yella, A.; Gao, P.; Humphry-Baker, R.; Curchod, B. F. E.; Ashari-Astani, N.; Tavernelli, I.; Rothlisberger, U.; Nazeeruddin, M. K.; Grätzel, M. Dye-Sensitized Solar Cells with 13% Efficiency Achieved through the Molecular Engineering of Porphyrin Sensitizers. *Nat. Chem.* **2014**, *6*, 242−247.

(10) Yao, Z.; Wu, H.; Li, Y.; Wang, J.; Zhang, J.; Zhang, M.; Guo, Y.; Wang, P. Dithienopicenocarbazole as the Kernel Module of Low-Energy-Gap Organic Dyes for Efficient Conversion of Sunlight to Electricity. *Energy Environ. Sci.* **2015**, *8*, 3192−3197.

(11) Kakiage, K.; Aoyama, Y.; Yano, T.; Oya, K.; Fujisawa, J.-i.; Hanaya, M. Highly-Efficient Dye-Sensitized Solar Cells with Collaborative Sensitization by Silyl-Anchor and Carboxy-Anchor Dyes. *Chem. Commun.* **2015**, *51*, 15894−15897.

(12) Chaurasia, S.; Liang, C.-J.; Yen, Y.-S.; Lin, J. T. Sensitizers with Rigidified-Aromatics as the Conjugated Spacers for Dye-Sensitized Solar Cells. *J. Mater. Chem. C* **2015**, *3*, 9765−9780.

(13) Ni, J.-S.; You, J.-H.; Hung, W.-I.; Kao, W.-S.; Chou, H.-H.; Lin, J. T. Organic Dyes Incorporating the Dithieno[3′,2′:3,4;2″,3″:5,6]-benzo[1,2-*c*]furazan Moiety for Dye-Sensitized Solar Cells. *ACS Appl. Mater. Interfaces* **2014**, *6*, 22612−22621.

(14) Ni, J.-S.; Kao, W.-S.; Chou, H.-J.; Lin, J. T. Organic Dyes Incorporating the Dithieno[3,2-*f*:2′,3′-*h*]quinoxaline Moiety for Dye-Sensitized Solar Cells. *ChemSusChem* **2015**, *8*, 2932−2939.

(15) Ni, J.-S.; Yen, Y.-C.; Lin, J. T. Organic Dyes with a Fused Segment Comprising Benzotriazole and Thieno[3,2-*b*]pyrrole Entities as the Conjugated Spacer for High Performance Dye-Sensitized Solar Cells. *Chem. Commun.* **2015**, *51*, 17080−17083.

(16) Ni, J.-S.; Yen, Y.-C.; Lin, J. T. Organic Sensitizers with a Rigid Dithienobenzotriazole-Based Spacer for High-Performance Dye-Sensitized Solar Cells. *J. Mater. Chem. A* **2016**, *4*, 6553−6560.

(17) Pai, R. K.; Ahipa, T. N.; Hemavathi, B. Rational Design of Benzodithiophene Based Conjugated Polymers for Better Solar Cell Performance. *RSC Adv.* **2016**, *6*, 23760−23774.

(18) Fan, Q.; Xu, Z.; Guo, X.; Meng, X.; Li, W.; Su, W.; Ou, X.; Ma, W.; Zhang, M.; Li, Y. High-Performance Nonfullerene Polymer Solar Cells with Open-Circuit Voltage Over 1 V and Energy Loss as Low As 0.54 eV. *Nano Energy* **2017**, *40*, 20−26.

(19) Fan, Q.; Su, W.; Meng, X.; Guo, X.; Li, G.; Ma, W.; Zhang, M.; Li, Y. High-Performance Non-Fullerene Polymer Solar Cells Based on Fluorine Substituted Wide Bandgap Copolymers Without Extra Treatments. *Solar RRL* **2017**, *1*, No. 1700020.

(20) Fan, Q.; Jiang, H.; Liu, Y.; Su, W.; Tan, H.; Wang, Y.; Yang, R.; Zhu, W. Efficient Polymer Solar Cells Based on A New Quinoxaline Derivative with Fluorinated Phenyl Side Chain. *J. Mater. Chem. C* **2016**, *4*, 2606−2613.

(21) Fan, Q.; Xiao, M.; Liu, Y.; Su, W.; Gao, H.; Tan, H.; Wang, Y.; Lei, G.; Yang, R.; Zhu, W. Improved Photovoltaic Performance of a 2D-Conjugated Benzodithiophene-Based Polymer by the Side Chain Engineering of Quinoxaline. *Polym. Chem.* **2015**, *6*, 4290−4298.

(22) Chen, S.; Jia, H.; Zheng, M.; Shen, K.; Zheng, H. Insight into the Effects of Modifying π-Bridges on the Performance of Dye-Sensitized Solar Cells Containing Triphenylamine Dyes. *Phys. Chem. Chem. Phys.* **2016**, *18*, 29555−29560.

(23) Gao, P.; Tsao, H. N.; Grätzel, M.; Nazeeruddin, M. K. Fine-Tuning the Electronic Structure of Organic Dyes for Dye-Sensitized Solar Cells. *Org. Lett.* **2012**, *14*, 4330−4333.

(24) Arroyave, F. A.; Richard, C. A.; Reynolds, J. R. Efficient Synthesis of Benzo[1,2-b:6,5-*b*′]dithiophene-4,5-dione (BDTD) and Its Chemical Transformations into Precursors for π-Conjugated Materials. *Org. Lett.* **2012**, *14*, 6138−6141.

(25) Huang, J.; Wang, X.; Zhang, X.; Niu, Z.; Lu, Z.; Jiang, B.; Sun, Y.; Zhan, C.; Yao, J. Additive-Assisted Control over Phase-Separated Nanostructures by Manipulating Alkylthienyl Position at Donor Backbone for Solution-Processed, Non-Fullerene, All-Small-Molecule Solar Cells. *ACS Appl. Mater. Interfaces* **2014**, *6*, 3853−3862.

(26) Kumar, C. V.; Cabau, L.; Koukaras, E. N.; Viterisi, A.; Sharma, G. D.; Palomares, E. Solution Processed Organic Solar Cells Based on A−D−D′−D−A Small Molecule with Benzo[1,2-*b*:4,5-*b*′]dithiophene Donor (D′) Unit, Cyclopentadithiophene Donor (D) and Ethyl-rhodanine Acceptor Unit Having 6% Light to Energy Conversion Efficiency. *J. Mater. Chem. A* **2015**, *3*, 4892−4902.

DOI: 10.1021/acsami.7b15181
ACS Appl. Mater. Interfaces 2017, 9, 43739−43746

(27) Chen, L.; Li, X.; Ying, W.; Zhang, X.; Guo, F.; Li, J.; Hua, J. 5,6-Bis(octyloxy)benzo[*c*][1,2,5]thiadiazole-Bridged Dyes for Dye-Sensitized Solar Cells with High Open-Circuit Voltage Performance. *Eur. J. Org. Chem.* **2013**, *2013*, 1770−1780.
(28) Chou, H.-H.; Chen, Y.-C.; Huang, H.-J.; Lee, T.-H.; Lin, J. T.; Tsai, C.; Chen, K. High-performance dye-sensitized solar cells based on 5,6-bis-hexyloxy-benzo[2,1,3]thiadiazole. *J. Mater. Chem.* **2012**, *22*, 10929−10938.
(29) Zhang, W.; Wu, Y.; Li, X.; Li, E.; Song, X.; Jiang, H.; Shen, C.; Zhang, H.; Tian, H.; Zhu, W.-H. Molecular Engineering and Sequential Cosensitization for Preventing the "Trade-off" Effect with Photovoltaic Enhancement. *Chem. Sci.* **2017**, *8*, 2115−2124.
(30) Wang, Y.; Zheng, Z.; Li, T.; Robertson, N.; Xiang, H.; Wu, W.; Hua, J.; Zhu, W.-H.; Tian, H. D−A−π−A Motif Quinoxaline-Based Sensitizers with High Molar Extinction Coefficient for Quasi-Solid-State Dye-Sensitized Solar Cells. *ACS Appl. Mater. Interfaces* **2016**, *8*, 31006−31024.
(31) Gao, Y.; Li, X.; Hu, Y.; Fan, Y.; Yuan, J.; Robertson, N.; Hua, J.; Marder, S. R. Effect of an Auxiliary Acceptor on D−A−π−A Sensitizers for Highly Efficient and Stable Dye-Sensitized Solar Cells. *J. Mater. Chem. A* **2016**, *4*, 12865−12877.
(32) Jradi, F. M.; Kang, X.; O'Neil, D.; Pajares, G.; Getmanenko, Y. A.; Szymanski, P.; Parker, T. C.; El-Sayed, M. A.; Marder, S. R. Near-Infrared Asymmetrical Squaraine Sensitized Solar Cells: The Effect of π-Bridges and Anchoring Groups on Solar Cells. *Chem. Mater.* **2015**, *27*, 2480−2487.
(33) Jradi, F. M.; O'Neil, D.; Kang, X.; Wong, J.; Szymanski, P.; Parker, T. C.; Anderson, H. L.; El-Sayed, M. A.; Marder, S. R. A Step Toward Efficient Pnachromatic Multi-Chromophoric Sensitizers for Dye-Sensitized Solar Cells. *Chem. Mater.* **2015**, *27*, 6305−6313.
(34) Daeneke, T.; Kwon, T.-H.; Holmes, A. B.; Duffy, N. W.; Bach, U.; Spiccia, L. High-Efficiency Dye-Sensitized Solar Cells with Ferrocene-Based Electrolytes. *Nat. Chem.* **2011**, *3*, 211−215.
(35) Wang, X.; Guo, L.; Xia, P. F.; Zheng, F.; Wong, M. S.; Zhu, Z. Dye-Sensitized Solar Cells Based on Organic Dyes with Naphtho[2,1-*b*:3,4-*b*′]dithiophene as the Conjugated Linker. *J. Mater. Chem. A* **2013**, *1*, 13328−13336.
(36) Dai, P.; Dong, H.; Liang, M.; Cheng, H.; Sun, Z.; Xue, S. Understanding the Role of Electron Donor in Truxene Dye Sensitized Solar Cells with Cobalt Electrolytes. *ACS Sustainable Chem. Eng.* **2017**, *5*, 97−104.
(37) Zhang, L.; Cole, J. M. Dye Aggregation in Dye-Sensitized Solar Cells. *J. Mater. Chem. A* **2017**, *5*, 19541−19559.
(38) Zhang, S.; Yang, X.; Qin, C.; Numata, Y.; Han, L. Interfacial Engineering for Dye-Sensitized Solar Cells. *J. Mater. Chem. A* **2014**, *2*, 5167−5177.
(39) Li, X.; Cui, S.; Wang, D.; Zhou, Y.; Zhou, H.; Hu, Y.; Liu, J.-g.; Long, Y.; Wu, W.; Hua, J.; Tian, H. New Organic Donor−Acceptor−π−Acceptor Sensitizers for Efficient Dye-Sensitized Solar Cells and Photocatalytic Hydrogen Evolution under Visible-Light Irradiation. *ChemSusChem* **2014**, *7*, 2879−2888.
(40) Thomas, K. R. J.; Hsu, Y.-C.; Lin, J. T.; Lee, K.-M.; Ho, K.-C.; Lai, C.-H.; Cheng, Y.-M.; Chou, P.-T. 2,3-Disubstituted Thiophene-Based Organic Dyes for Solar Cells. *Chem. Mater.* **2008**, *20*, 1830−1840.
(41) Qu, S.; Qin, C.; Islam, A.; Hua, J.; Chen, H.; Tian, H.; Han, L. Tuning the Electrical and Optical Properties of Diketopyrrolopyrrole Complexes for Panchromatic Dye-Sensitized Solar Cells. *Chem. − Asian J.* **2012**, *7*, 2895−2903.
(42) Hara, K.; Sato, T.; Katoh, R.; Furube, A.; Ohga, Y.; Shinpo, A.; Suga, S.; Sayama, K.; Sugihara, H.; Arakawa, H. Molecular Design of Coumarin Dyes for Efficient Dye-Sensitized Solar Cells. *J. Phys. Chem. B* **2003**, *107*, 597−606.
(43) Ying, W.; Yang, J.; Wielopolski, M.; Moehl, T.; Moser, J.-E.; Comte, P.; Hua, J.; Zakeeruddin, S. M.; Tian, H.; Grätzel, M. New Pyrido[3,4-*b*]pyrazine-Based Sensitizers for Efficient and Stable Dye-Sensitized Solar Cells. *Chem. Sci.* **2014**, *5*, 206−214.
(44) Li, H.; Wu, Y.; Geng, Z.; Liu, J.; Xu, D.; Zhu, W. Co-Sensitization of Benzoxadiazole Based D−A−π−A Featured Sensitizers: Compensating Light Harvesting and Retarding Charge Recombination. *J. Mater. Chem. A* **2014**, *2*, 14649−14657.
(45) Manthou, V. S.; Pefkianakis, E. K.; Falaras, P.; Vougioukalakis, G. C. Co-Adsorbents: A Key Component in Efficient and Robust Dye-Sensitized Solar Cells. *ChemSusChem* **2015**, *8*, 588−599.
(46) Li, L.-L.; Chang, Y.-C.; Wu, H.-P.; Diau, E. W.-G. Characterisation of Electron Transport and Charge Recombination Using Temporally Resolved and Frequency-Domain Techniques for Dye Sensitized Solar Cells. *Int. Rev. Phys. Chem.* **2012**, *31*, 420−467.
(47) Wang, M.; Grätzel, C.; Zakeeruddin, S. M.; Grätzel, M. Recent Developments in Redox Electrolytes for Dye-Sensitized Solar Cells. *Energy Environ. Sci.* **2012**, *5*, 9394−9405.
(48) Sun, Z.; Liang, M.; Chen, J. Kinetics of Iodine-Free Redox Shuttles in Dye-Sensitized Solar Cells: Interfacial Recombination and Dye Regeneration. *Acc. Chem. Res.* **2015**, *48*, 1541−1550.
(49) Li, C.-T.; Wu, F.-L.; Liang, C.-J.; Ho, K.-C.; Lin, J. T. Effective Suppression of Interfacial Charge Recombination by a 12-Crown-4 Substituent on a Double-Anchored Organic Sensitizer and Rotating Disk Electrochemical Evidence. *J. Mater. Chem. A* **2017**, *5*, 7586−7594.
(50) Li, L.-L.; Diau, E. W.-G. Porphyrin-Sensitized Solar Cells. *Chem. Soc. Rev.* **2013**, *42*, 291−304.

DOI: 10.1021/acsami.7b15181
ACS Appl. Mater. Interfaces 2017, 9, 43739−43746